Efficient Monte Carlo Device Modeling

F. M. Bufler, A. Schenk, and Wolfgang Fichtner, *Fellow, IEEE*

Abstract—A single-particle approach to full-band Monte Carlo device simulation is presented which allows an efficient computation of drain, substrate and gate currents in deep submicron MOSFETs. In this approach, phase-space elements are visited according to the distribution of real electrons. This scheme is well adapted to a test-function evaluation of the drain current, which emphasizes regions with large drift velocities (i.e., in the inversion channel), a substrate current evaluation via the impact ionization generation rate (i.e., in the LDD region with relatively high electron temperature and density) and a computation of the gate current in the dominant direct-tunneling regime caused by relatively cold electrons (i.e., directly under the gate at the source well of the inversion channel). Other important features are an efficient treatment of impurity scattering, a phase-space steplike propagation of the electron allowing to minimize self-scattering, just-before-scattering gathering of statistics, and the use of a frozen electric field obtained from a drift-diffusion simulation. As an example an 0.1-μm n-MOSFET is simulated where typically 30 minutes of CPU time are necessary per bias point for practically sufficient accuracy.

Index Terms—Boltzmann equation, hot carriers, Monte Carlo methods, MOSFETs, semiconductor device modeling.

I. INTRODUCTION

A S THE downscaling of MOSFET devices continues, the number of scattering events suffered by electrons while traveling through the channel is more and more reduced. This leads to quasiballistic and nonlocal transport, where the distribution function strongly deviates from its equilibrium shape, and this effect will become even more pronounced when channel lengths are scaled into the sub-0.1-μm regime in the next decade. Therefore knowledge of the distribution function, which is obtained from a solution of the Boltzmann transport equation (BTE), is of major importance for an accurate determination of drain, substrate, and gate currents in the nonlinear operation regime of future MOSFETs.

An exact solution of the BTE can be obtained by the Monte Carlo (MC) method [1], [2], where the acceleration of electrons through the electric field as well as the scattering by phonons, impurities, etc., are simulated, and quantities of interest result from averaging over microscopic variables such as the particle energy. The accuracy of the semiclassical transport description is then given by the models used for the band structure and the scattering mechanisms. In this respect, it has been found that the consideration of the full band structure as obtained from the empirical pseudopotential method [3], [4] is indispensable for a re-

liable description of nonlocal transport phenomena and hot-carrier effects dominant in the submicron regime [5]–[7]. Explicit comparisons between full-band and analytical band structure descriptions have shown the in part strong limitations of the analytical approach in bulk material for the high-energy distribution [8] and the drift velocity [9] in Si as well as on the device level for the simulation of GaAs MESFETs [10].

However, many implementations of Monte Carlo simulators involve large computation times which are usually not affordable in technology development. Therefore, alternative approaches to the solution of the BTE have been developed which essentially aim at trading memory requirements for computational speed. These alternatives are the concept of cellular automata (CA) [11]–[15], where the distribution function is stored in each real-space element of the device and evolves in time by spatially local rules, the scattering matrix approach (SMA) [16]–[19], where precomputed scattering matrices relate incoming and outgoing fluxes of semiconductor elements, and the spherical-harmonics expansion (SHE) of the BTE [20]–[23], which transforms the BTE in a system of equations for the expansion coefficients. On the other hand, apart from considerable memory requirements, device simulations based on the above approaches mostly rely on analytical band structure descriptions or take only reduced full-band aspects into account neglecting, e.g., the anisotropy of the group velocity. In contrast, full-band Monte Carlo (FBMC) device simulations of Si MOSFETs are state-of-the-art [6], [24]–[29].

This suggests as another possibility for an efficient solution of the BTE including full-band effects to retain the accuracy, simplicity and flexibility of the Monte Carlo approach and to improve the computational efficiency of FBMC device simulation. Progress in this direction has been achieved by using the frozen field from a drift-diffusion simulation [30], through the reduction of self-scattering by propagating the electrons steplike in phase-space [31] and by an efficient choice of the state-after-scattering [29], but the most efficient applications have so far been restricted to substrate current calculations [26].

It is the aim of this paper to present a full-band MC approach that allows us to compute drain, substrate and gate currents with similar efficiency and includes additional improvements of the MC algorithm to further enhance the computational speed of FBMC device simulation. On one hand, this is achieved by a single-particle approach (SPARTA), where only a single electron is simulated at a time, which carries the charge of all charge carriers in the device. It exploits the fact that in deep submicron MOSFETs under normal bias conditions the concentration of real electrons in phase-space is rather high in regions which are relevant for the computation of drain, substrate and gate currents when using appropriate current estimators. On the other hand, the progress in efficiency is due to improvements of the MC al-

gorithm based on the self-scattering scheme and the phase-space steplike trajectory calculation including an efficient treatment of impurity scattering.

II. MONTE CARLO MODEL

In this section, the underlying physical models as well as various parts of the Monte Carlo algorithm are explained. Emphasis is laid on new aspects which are crucial for the computational performance. Other points are only briefly addressed with reference to the literature. Since the example for device simulation in this paper is an n-MOSFET, only the models for electrons are described and those for the holes are left out.

A. Models for Band Structure and Scattering Mechanisms

The full band structure for Si is obtained by nonlocal pseudopotential calculations [32], where, in addition, the spin-orbit interaction is taken into account [33]. Four conduction bands are stored on a mesh in momentum-space with an equidistant grid-spacing of $1/64 \, 2\pi/a_0$, where a_0 denotes the lattice constant. Within each cube the band energy is expanded to linear order around the middle of the cube. Hence, the group velocity is constant in each momentum-space element.

The scattering mechanisms comprise phonon scattering, impact ionization, impurity scattering, and surface roughness scattering. The phonon scattering model includes three g-type and three f-type intervalley processes as well as intravalley scattering in the elastic equipartition approximation [1]. The coupling constants of [1] are only multiplied by a global factor of 0.98 to account for band structure differences [33]. The scattering rate for impact ionization is taken from [34].

Impurity scattering is important in MOSFETs because of the highly doped source and drain contacts [35]. Unfortunately, it is also computationally intensive due to high scattering rates at low energies while almost not changing the momentum. This effect is particularly strong in the Brooks–Herring (BH) model, which describes the screened two-body interaction with one ionized impurity [36]. It is reduced in the statistical screening model of Ridley (RI) considering the probability that there is no nearer scattering center [37]. The most significant reduction of the computational burden, however, is achieved by approximating the scattering rate by the inverse microscopic relaxation time and selecting the state-after-scattering at random on the equienergy surface. This can be seen in Fig. 1 where for purposes of illustration density and doping concentration have been chosen such that this effect is particularly pronounced. Comprehensive investigations [38], [39] have shown that there is also at high fields almost no difference between this approximation and the exact treatment. Since impurity scattering is only important at low energies, an analytic isotropic and nonparabolic band structure is used for the calculation of the inverse microscopic relaxation time up to 0.5 eV neglecting impurity scattering for higher electron energies. The inverse relaxation time is given by

$$\frac{1}{\tau_{\mathrm{RI}}(\epsilon)} = \frac{V}{(2\pi)^3} \int d^3k' S_{\mathrm{RI}}\left(\boldsymbol{k}'|\boldsymbol{k}\right)\left(1 - \hat{\boldsymbol{k}}' \cdot \hat{\boldsymbol{k}}\right) \quad (1)$$
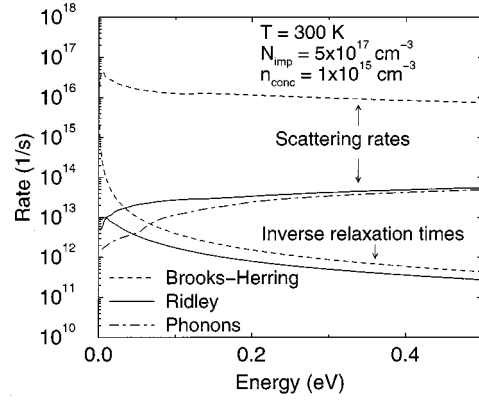

Fig. 1. Scattering rates and inverse microscopic relaxation times of impurity scattering in the formulation of Brooks–Herring and Ridley. The phonon scattering rate is shown for comparison.

where V denotes the crystal volume, $S_{\mathrm{RI}}(\boldsymbol{k}'|\boldsymbol{k})$ the transition probability per unit time and $\hat{\boldsymbol{k}} = \boldsymbol{k}/|\boldsymbol{k}|$. The result is

$$\frac{1}{\tau_{\mathrm{RI}}(\epsilon)} = F \left\{ \exp\left(\frac{aF}{2v}\frac{\eta}{1+\eta}\right) \right.$$
$$\times \left[\mathrm{Ei}\left(-\frac{aF}{2v}\eta\right) - \mathrm{Ei}\left(-\frac{aF}{2v}\frac{\eta}{1+\eta}\right) \right]$$
$$\left. - \frac{2v}{aF}\frac{1}{\eta}\left[1 - \exp\left(-\frac{aF}{2v}\frac{\eta^2}{1+\eta}\right)\right] \right\} \quad (2)$$

with the following abbreviations:

$$F(\epsilon) = \frac{\pi e^4 N_{\mathrm{imp}}}{(4\pi\varepsilon)^2\sqrt{2m_{\mathrm{d}}}} \times \frac{1 + 2\alpha\epsilon}{(\epsilon(1+\alpha\epsilon))^{3/2}} \quad (3)$$

$$\eta(\epsilon) = \frac{8m_{\mathrm{d}}\epsilon(1+\alpha\epsilon)}{\hbar^2\beta^2} \quad (4)$$

$$v(\epsilon) = \sqrt{\frac{2}{3\,m_{\mathrm{cond}}}} \times \frac{\sqrt{\epsilon(1+\alpha\epsilon)}}{1 + 2\alpha\epsilon}. \quad (5)$$

Here, e is the elementary charge, N_{imp} the impurity concentration, ε the static dielectric constant of Si, m_{d} the density-of-states mass at the band edge, α the nonparabolicity factor, $\beta = \sqrt{e^2 n/(\varepsilon k_B T)}$ the inverse screening length (n denotes the electron density, k_B the Boltzmann constant and T the lattice temperature), $a = (2\pi N_{\mathrm{imp}})^{-1/3}$ the mean distance between impurities, and $\mathrm{Ei}(x) = \int_{-\infty}^{x} dt\, e^t/t$ the exponential integral. Because the velocity v enters ad hoc the relation between the scattering rates of the BH and the RI model [40], we have used the conductivity mass m_{cond} of the anisotropic analytic band model [1] as the most plausible choice in (5). Since the ohmic drift mobility with the above impurity scattering model significantly deviates especially for high doping concentrations from the experimental results, a doping-dependent prefactor is introduced in (2) to reproduce the mobility measurements of [41]. This approach to impurity scattering is admittedly rather heuristic, but it correctly and efficiently accounts for the two main effects, i.e., the mobility reduction in the highly doped contact regions and the screening in the inversion channel. Effects due to the finite number of dopants are not included, because this paper aims primarily at the investigation of the nonlinear and hot-electron regime under inversion
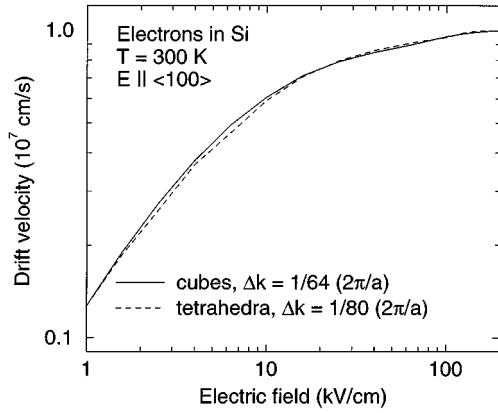
Fig. 2. Influence of the k-space discretization on the velocity-field characteristics in undoped Si.

conditions, whereas dopant fluctuations have their main consequences near the threshold voltage. For random dopant-induced problems and their suppression see the recent literature [42], [43] and references therein.

Surface roughness scattering is treated phenomenologically by randomly selecting either a reflective or a diffusive scattering process when an electron hits the surface to the oxide. The probability for diffusive scattering is chosen such that the drain current of the drift-diffusion simulation is reproduced in the linear regime [27]. This is in order to ensure the consistency of the underlying transport models since in practice the surface contribution of the mobility of the drift-diffusion model must often itself be adjusted for a given technology.

B. Trajectory Calculation

Along the lines developed in [31] the time during which the electron is propagated according to Newton's law is determined as the minimum of four times: i) the flight time to reach the border of the three-dimensional momentum-space element, ii) the flight time to reach the border of the two-dimensional real-space element, iii) the remaining time to the end of a time interval into which the whole simulation time is divided where, e.g., simulation results are stored and iv) the stochastically selected time for a scattering event. Since momentum-space changes occur rather often, the relatively coarse and equidistant tensor grid in momentum space is very beneficial for the calculation of the intersection with the border of a momentum-space element. Fig. 2 compares the velocity-field characteristic in bulk Si simulated with the present mesh of cubes to the result of a finer mesh of tetrahedra with a spacing of $1/80\ 2\pi/a_0$ using exactly the same physical model [33, Fig. 5.25, p. 119]. It can be seen that the discretization error is rather small. In addition, the comparison in Fig. 2 confirms the validity of the present approach because a different MC algorithm was employed in [33].

This kind of trajectory calculation involves several advantages. Above all, it allows within the scheme of self-scattering the use of different and rather small upper estimates of the real scattering rates in each phase-space element. For the energy-dependent scattering rates of phonon scattering and impact ion-

ization, an upper estimation is computed and stored for each momentum-space element. The corresponding rate for impurity scattering in (2) depends in addition on the impurity concentration N_{imp} and the electron density n. Therefore, an upper estimation is determined and stored for each real-space element using the density obtained by the drift-diffusion simulation. An aspect critical for the CPU time within the self-scattering scheme is the costly computation of the logarithm for the free flight time. This can mostly be avoided by first considering the probability P_3 that (real or fictitious) scattering occurs before the other three events

$$P_3 = 1 - e^{-\Gamma t_3} \tag{6}$$

where Γ is the upper estimate of the real scattering rate and t_3 the minimum of the times for the electron to leave the momentum-space element, to leave the real-space element and to reach the end of the given time interval. Hence, the collisionless time-of-flight t_{f} needs only to be computed if an equally between zero and one selected random number r is smaller than P_3 and is then given by

$$t_{\text{f}} = -\frac{1}{\Gamma} \ln(1 - r). \tag{7}$$

Another advantage is the simple integration of Newton's equations of motion since the group velocity is constant in a momentum-space element and also a constant electric field, taken from the drift-diffusion simulation, is assigned to a real-space element. However, an additional action is required for Newton's equations because the channel in MOSFETs, i.e., the corresponding line from source to drain, is oriented along the crystallographic $\langle 110 \rangle$ direction, but the crystal momentum in the band structure calculation refers to a coordinate system with the coordinate axes parallel to the principal axes of Si (note that this discussion does *not* refer to the growth direction of the wafer, which is in z-direction, but to the direction within the xy-plane parallel to the Si/SiO$_2$ interface). Under the orthogonal transformation $\boldsymbol{k}' = \mathcal{U}\boldsymbol{k}$, where $\boldsymbol{k}'$ refers to the Cartesian frame aligned with the principal axes, the equations of motion become

$$\frac{d}{dt}\boldsymbol{k}' = -\frac{e}{\hbar}\mathcal{U}\boldsymbol{E}(\boldsymbol{r}) \tag{8}$$

$$\frac{d}{dt}\boldsymbol{r} = \mathcal{U}^T\boldsymbol{v}'\left(\boldsymbol{k}'\right) \tag{9}$$

with the transformation matrix

$$\mathcal{U} = \begin{pmatrix} a & b & 0 \\ -b & a & 0 \\ 0 & 0 & 1 \end{pmatrix} \tag{10}$$

where $a = b = 1/\sqrt{2}$. This transformation must also be invoked for the surface roughness scattering process.

A further advantage is the possibility to restrict computational actions to the necessary cases only, e.g., updating the group velocity of a particle only when the momentum-space element is left or accessing the table with the real scattering rates only when a scattering process is to be performed.

Finally, the selection of the state-after-scattering is modeled with linked lists in the spirit of [29]. All cubes of the irreducible wedge of the Brillouin zone are stored in a list of energy intervals when having a common energy range. The energy after scattering determines a corresponding energy interval of the list and a cube is selected according to its partial density of states by the acceptance-rejection technique [1] with a constant upper estimation of the partial densities of states of all cubes in this energy interval. The momentum-after-scattering is then stochastically chosen on the equienergy plane in this cube.

C. Single-Particle Approach and Boundary Conditions

In SPARTA, a single electron is simulated in the frozen electric field as obtained for each bias point from the classical drift-diffusion simulation. The frozen-field approach [30] relies on the plausible assumption that the details of the distribution function arising from nonlocal and hot-electron effects do not significantly influence the electric field. While the ultimate limit of this approach remains to be explored, explicit investigations of deep submicron n-MOSFETs [26] have shown that the differences in the electrostatic potential profiles as obtained from self-consistent MC simulations and classical device simulations are in fact negligible. We have therefore adopted this approach extending it to a frozen-total-charge approach where the single electron is assigned the charge of all electrons in the device as given by the solution of the drift-diffusion simulation allowing, of course, still a different spatial dependence of the electron density. All phase-space elements are visited by the single electron according to the distribution of the real electrons and as a consequence unimportant regions such as the bulk region are not simulated at all. The computational burden of the highly doped contact regions is no longer a problem due to the efficient treatment of impurity scattering as described above.

The ohmic boundary conditions at the contacts are addressed by an ensemble MC simulation as introduced by Peifer [44]. Equally weighted particles are distributed to the contact elements according to the equilibrium density. During the simulation a particle in a contact element cannot leave the contact element. When it hits a border, it is put at the opposite side of the element and, if the border is with the active device, a single-particle is injected. This single-particle is simulated until it hits a contact element where it is absorbed and a new ensemble simulation in all contact elements is started. Secondary particles generated by impact ionization are neglected in this approach. Situations such as occurring in SOI MOSFETs, where the generated particles influence the device behavior significantly, can therefore not be treated by SPARTA, but require an ensemble Monte Carlo simulation instead.

D. Gathering of Statistics

During the simulation, cumulative expectation values of microscopic quantities, such as the group velocity, the energy, or the impact ionization scattering rate, are collected in each real-space element. Usually, this is done at equidistant time steps

of the simulation, but this is rather CPU time consuming if the time step is small. We therefore gather statistics at times just-before-scattering [1]. Within the scheme of phase-space-element depending upper estimations of the real scattering rate, the expectation value of a microscopic quantity A is given by

$$\langle A \rangle_r = \frac{\sum_{i,\, \boldsymbol{r}(t_i) \in r} \Gamma_{r,k_i}^{-1} A\left(\boldsymbol{k}(t_i)\right)}{\sum_{i,\, \boldsymbol{r}(t_i) \in r} \Gamma_{r,k_i}^{-1}} \qquad (11)$$

where the sum runs over the times t_i of scattering events in the real-space element r. k_i denotes the momentum-space element occupied before t_i and $\Gamma_{r,k}^{-1}$ is the inverse upper estimation in the phase-space element (r, k). In addition, since a single-particle simulation is performed, gathering of statistics can begin with the start of the simulation without the need to reach a stationary state before as is necessary in an ensemble simulation.

III. ESTIMATORS FOR CURRENTS

This section briefly explains how estimations for drain, substrate, and gate currents are obtained and addresses the associated advantages within the single-particle approach. Note that they consist not only of the relatively high population of the relevant phase-space, but also of the simple general algorithm which especially does not require the computational effort of statistical enhancement techniques.

A. Drain Current

The drain current I_{D} is estimated with the test-function method proposed by Yoder [45], [46]. Densities and drift velocities entering the optimization of the test functions [46] are initially taken from the drift-diffusion solution and replaced by Monte Carlo results when the real-space element has been visited by the particle. This methods emphasizes regions with high drift velocities, i.e., at the drain side of the inversion channel [46]. This is also a region with high density, i.e., often visited within the single-particle approach, and with high electron temperature, which involves high scattering rates and hence many scattering events for gathering statistics within the just-before-scattering method.

B. Substrate Current

The substrate current I_{S} is calculated via the expectation value of the impact ionization scattering rate S_{II} according to

$$I_{\mathrm{S}} = e, \int d^2r\; n(\boldsymbol{r}) \langle S_{\mathrm{II}} \rangle(\boldsymbol{r}) \qquad (12)$$

where the integration is over the whole two-dimensional (2-D) device. Note that this formula only holds when all generated holes can be assumed to leave the device via the substrate contact. Impact ionization occurs mainly in the lowly-doped-drain (LDD) region near the channel where again electron density and electron temperature are rather high leading to enhanced scattering and hence improved statistics.
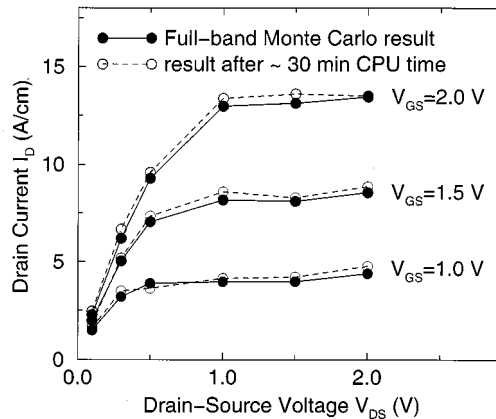
Fig. 3.   Full-band Monte Carlo simulation of drain current characteristics in an 0.1 μm n-MOSFET with 3 nm oxide thickness for three gate voltages.

C. Gate Current

The gate current I_G is given by

$$I_G = e \int dx\, n(\boldsymbol{r}) \tfrac{1}{2} \left\langle |\hat{\boldsymbol{n}} \cdot \boldsymbol{v}|\, T \right\rangle (\boldsymbol{r}) \qquad (13)$$

where the one-dimensional (1-D) integration is along the gate oxide. Here, $\hat{n}$ is the unit vector normal to the gate oxide and T denotes the tunneling probability obtained via the WKB approximation for a trapezoidal shape of the barrier. For the low supply voltages of deep submicron MOSFETs, gate currents are dominantly due to direct tunneling of relatively cold electrons near the source side of the inversion channel [47], where the electron density is high. This is again advantageous for the current estimation.

IV. SIMULATION RESULTS

The performance of the MC algorithm presented is investigated by a simulation of an LDD n-MOSFET with an effective gate length of 0.1 μm and an oxide thickness of 3 nm. The real-space mesh consists of triangles and rectangles and comprises 1987 elements. Typically, sufficient accuracy is achieved after 0.6-μs simulation time per bias point which corresponds to 30 min CPU time on a 500 MHz DEC AlphaServer 21 264. In order to illustrate the accuracy obtained after 30 min CPU time in a simple and comprehensive overview for all currents, the results are compared to long MC simulations of 30-μs simulation time with negligible variance. The corresponding characteristics at room temperature for drain, substrate and gate currents are displayed in Figs. 3–5, respectively. It can be seen that indeed sufficient accuracy is reached after 30 min CPU time in all cases except for the substrate current at the lowest drain voltage. Most remarkable is the fact that similar accuracy is obtained for all three currents after the same simulation time. This will enable important consistency checks in practical applications.

V. CONCLUSIONS

A single-particle approach to full-band MC device simulation based on the frozen-field approximation has been pre-
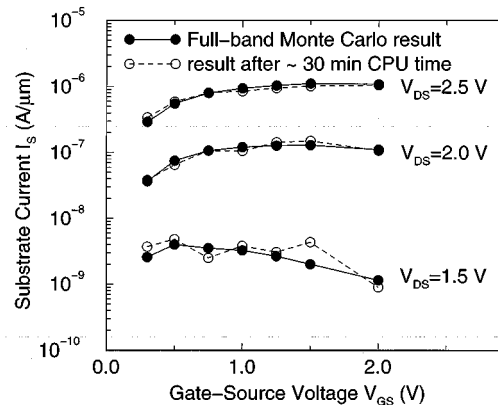

Fig. 4.   Full-band Monte Carlo simulation of substrate current characteristics in an 0.1 μm n-MOSFET with 3-nm oxide thickness for three drain voltages.
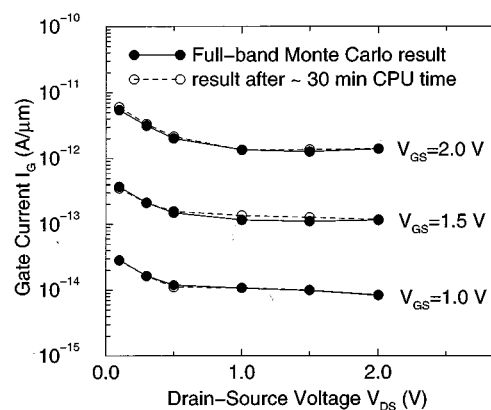

Fig. 5.   Full-band Monte Carlo simulation of gate current characteristics in an 0.1 μm n-MOSFET with 3-nm oxide thickness for three gate voltages.

sented. Its efficiency was demonstrated by the simulation of an 0.1-μm n-MOSFET where 30 min of CPU time per bias point were sufficient for the calculation of drain, substrate and gate current. The approach takes advantage of the relatively high distribution of carriers in phase-space regions, which are relevant for the current estimators, and includes several improvements of a phase-space steplike MC algorithm and the treatment of impurity scattering. Due to the capability to incorporate ballistic and hot-carrier effects and with the efficiency achieved, full-band MC simulation can be expected to become an integral part of the device simulation techniques for sub 0.1-μm MOSFETs.

REFERENCES

[1] C. Jacoboni and L. Reggiani, "The Monte Carlo method for the solution of charge transport in semiconductors with application to covalent materials," *Rev. Mod. Phys.*, vol. 55, pp. 645–705, 1983.
[2] C. Jacoboni and P. Lugli, *The Monte Carlo Method for Semiconductor Device Simulation.*   Berlin, Germany: Springer, 1989.
[3] J. R. Chelikowsky and M. L. Cohen, "Nonlocal pseudopotential calculations for the electronic structure of eleven diamond and zinc-blende semiconductors," *Phys. Rev. B*, vol. 14, pp. 556–582, 1976.

[4] M. L. Cohen and J. R. Chelikowsky, *Electronic Structure and Optical Properties of Semiconductors*, 2nd ed. Berlin, Germany: Springer, 1989.

[5] H. Shichijo and K. Hess, "Band-structure-dependent transport and impact ionization in GaAs," *Phys. Rev. B*, vol. 23, pp. 4197–4207, 1991.

[6] M. V. Fischetti and S. E. Laux, "Monte Carlo analysis of electron transport in small semiconductor devices including band-structure and space-charge effects," *Phys. Rev. B*, vol. 38, pp. 9721–9745, 1988.

[7] K. Hess, Ed., *Monte Carlo Device Simulation: Full Band and Beyond*. Boston, MA: Kluwer, 1991.

[8] C. Jungemann, S. Keith, F. M. Bufler, and B. Meinerzhagen, "Effects of band structure and phonon models on hot electron transport in silicon," *Elec. Eng.*, vol. 79, pp. 99–101, 1996.

[9] F. M. Bufler, P. Graf, S. Keith, and B. Meinerzhagen, "Full band Monte Carlo investigation of electron transport in strained Si grown on $Si_{1-x}Ge_x$ substrates," *Appl. Phys. Lett.*, vol. 70, pp. 2144–2146, 1997.

[10] Y. Ando, W. Contrata, Y. Hori, and N. Samoto, "Monte Carlo simulation for electron transport in MESFET's including realistic band structure of GaAs," *IEEE Electron Device Lett.*, vol. 20, pp. 454–456, 1999.

[11] K. Kometer, G. Zandler, and P. Vogl, "Lattice-gas cellular-automaton method for semiclassical transport in semiconductors," *Phys. Rev. B*, vol. 46, pp. 1382–1394, 1992.

[12] G. Zandler *et al.*, "A comparison of Monte Carlo and cellular automata approaches for semiconductor device simulation," *IEEE Electron Device Lett.*, vol. 14, pp. 77–79, 1993.

[13] M. Saraniti *et al.*, "Cellular automata simulation of nanometer-scale MOSFETs," *Semicond. Sci. Technol.*, vol. 13, pp. A177–A179, 1998.

[14] K. Fukuda and K. Nishi, "An interpolated flux scheme for cellular automaton device simulation," *IEEE Trans. Computer-Aided Design*, vol. 17, pp. 553–560, 1998.

[15] M. Saraniti and S. M. Goodnick, "A full-band cellular automaton for charge transport simulation in semiconductors," in *Proc. IWCE*, Osaka, Japan, Oct. 1998, pp. 88–91.

[16] A. Das and M. S. Lundstrom, "A scattering matrix approach to device simulation," *Solid-State Electron.*, vol. 33, pp. 1299–1307, 1990.

[17] M. A. Alam, M. A. Stettler, and M. S. Lundstrom, "Formulation of the Boltzmann equation in terms of scattering matrices," *Solid-State Electron.*, vol. 36, pp. 263–271, 1993.

[18] A. Das and M. S. Lundstrom, "Scattering matrix simulation of electron transport in model bipolar devices," *IEEE Trans. Electron Devices*, vol. 39, pp. 1157–1163, 1992.

[19] Z. Han, N. Goldsman, and M. A. Stettler, "The realization of scattering matrix approach to transport modeling through spherical harmonics," *Solid-State Electron.*, vol. 43, pp. 493–501, 1999.

[20] K. A. Hennacy, Y.-J. Wu, N. Goldsman, and I. D. Mayergoyz, "Deterministic MOSFET simulation using a generalized spherical harmonic expansion of the Boltzmann equation," *Solid-State Electron.*, vol. 38, pp. 1485–1495, 1995.

[21] M. C. Vecchi, J. Mohring, and M. Rudan, "An efficient solution scheme for the spherical-harmonics expansion of the Boltzmann transport equation," *IEEE Trans. Computer-Aided Design*, vol. 16, pp. 353–361, 1997.

[22] M. C. Vecchi and M. Rudan, "Modeling electron and hole transport with full-band structure effects by means of the spherical-harmonics expansion of the BTE," *IEEE Trans. Electron Devices*, vol. 45, pp. 230–238, 1998.

[23] S. Reggiani, M. C. Vecchi, and M. Rudan, "Investigation on electron and hole transport properties using the full-band spherical-harmonics expansion method," *IEEE Trans. Electron Devices*, vol. 45, pp. 2010–2017, 1998.

[24] J. D. Bude and M. Mastrapasqua, "Impact ionization and distribution functions in sub-micron nMOSFET technologies," *IEEE Electron Device Lett.*, vol. 16, pp. 439–441, 1995.

[25] N. Sano, M. Tomizawa, and A. Yoshii, "Temperature dependence of hot carrier effects in short-channel Si-MOSFET's," *IEEE Trans. Electron Devices*, vol. 42, pp. 2211–2116, 1995.

[26] C. Jungemann, S. Yamaguchi, and H. Goto, "On the accuracy and efficiency of substrate current calculations for sub-μm n-MOSFET's," *IEEE Electron Device Lett.*, vol. 17, pp. 464–466, 1996.

[27] S. E. Laux and M. V. Fischetti, "Monte Carlo study of velocity overshoot in switching a 0.1-micron CMOS inverter," in *IEDM Tech. Dig.*, 1997, pp. 877–880.

[28] A. Duncan, U. Ravaioli, and J. Jakumeit, "Full-band Monte Carlo investigation of hot carrier trends in the scaling of metal-oxide-semiconductor field-effect transistors," *IEEE Trans. Electron Devices*, vol. 45, pp. 867–876, 1998.

[29] C. Jungemann, S. Keith, M. Bartels, and B. Meinerzhagen, "Efficient full-band Monte Carlo simulation of silicon devices," *IEICE Trans. Electron.*, vol. E82-C, pp. 870–879, 1999.

[30] J. M. Higman, K. Hess, C. G. Hwang, and R. W. Dutton, "Coupled Monte Carlo-drift diffusion analysis of hot-electron effects in MOSFET's," *IEEE Trans. Electron Devices*, vol. 36, pp. 930–937, 1989.

[31] J. Bude and R. K. Smith, "Phase-space simplex Monte Carlo for semiconductor transport," *Semicond. Sci. Technol.*, vol. 9, pp. 840–843, 1994.

[32] M. M. Rieger and P. Vogl, "Electronic-band parameters in strained $Si_{1-x}Ge_x$ alloys on $Si_{1-y}Ge_y$ substrates," *Phys. Rev. B*, vol. 48, pp. 14 276–14 287, 1993.

[33] F. M. Bufler, *Full-Band Monte Carlo Simulation of Electrons and Holes in Strained Si and SiGe*. Munich, Germany: Herbert Utz Verlag, 1998.

[34] E. Cartier, M. V. Fischetti, E. A. Eklund, and F. R. McFeely, "Impact ionization in silicon," *Appl. Phys. Lett.*, vol. 62, pp. 3339–3341, 1993.

[35] F. M. Bufler, P. D. Yoder, and W. Fichtner, "Simple phase-space trajectory calculation for Monte Carlo device simulation including screened impurity scattering," in *Proc. SISPAD*, Kyoto, Japan, Sept. 1999, pp. 31–34.

[36] H. Brooks, "Scattering by ionized impurities in semiconductors," *Phys. Rev.*, vol. 83, p. 879, 1951.

[37] B. K. Ridley, "Reconciliation of the Conwell–Weisskopf and Brooks–Herring formulae for charged-impurity scattering in semiconductors: Third-body interference," *J. Phys. C*, vol. 10, pp. 1589–1593, 1977.

[38] P. Graf, *Entwicklung eines Monte-Carlo-Bauelementsimulators für Si/SiGe-Heterobipolartransistoren*. Munich, Germany: Herbert Utz Verlag, 1999.

[39] H. Kosina, "A method to reduce small-angle scattering in Monte Carlo device analysis," *IEEE Trans. Electron Devices*, vol. 46, pp. 1196–1200, 1999.

[40] T. G. V. de Roer and F. P. Widdershoven, "Ionized impurity scattering in Monte Carlo calculations," *J. Appl. Phys.*, vol. 59, pp. 813–815, 1986.

[41] G. Masetti, M. Severi, and S. Solmi, "Modeling of carrier mobility against carrier concentration in arsenic-, phosphorus-, and boron-doped silicon," *IEEE Trans. Electron Devices*, vol. 30, pp. 764–769, 1983.

[42] A. Asenov, A. R. Brown, J. H. Davies, and S. Saini, "Hierarchical approach to "atomistic" 3-D MOSFET simulation," *IEEE Trans. Computer-Aided Design*, vol. 18, pp. 1558–1565, 1999.

[43] A. Asenov and S. Saini, "Suppression of random dopant-induced threshold voltage fluctuations in sub-0.1 μm MOSFET's with epitaxial and δ-doped channels," *IEEE Trans. Electron Devices*, vol. 46, pp. 1718–1724, 1999.

[44] H.-J. Peifer, "Monte-Carlo-Simulation des Hochenergietransportes von Elektronen," in *MOS-Strukturen*. Aachen, Germany: Augustinus-Buchhandlung, 1992.

[45] P. D. Yoder, K. Gärtner, and W. Fichtner, "A generalized Ramo–Shockley theorem for classical to quantum transport at arbitrary frequencies," *J. Appl. Phys.*, vol. 79, pp. 1951–1954, 1996.

[46] P. D. Yoder, K. Gärtner, U. Krumbein, and W. Fichtner, "Optimized terminal current calculation for Monte Carlo device simulation," *IEEE Trans. Computer-Aided Design*, vol. 16, pp. 1082–1087, 1997.

[47] E. Cassan, S. Galdin, P. Dollfus, and P. Hesto, "Study of direct tunneling through ultrathin gate oxide of field effect transistors using Monte Carlo simulation," *J. Appl. Phys.*, vol. 86, pp. 3804–3811, 1999.
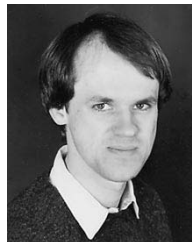
F. M. Bufler studied physics at the Technical University Braunschweig, Germany, and RWTH Aachen, Germany, including an academic year at the Université de Grenoble I (France) with a scholarship of the Studienstiftung des Deutschen Volkes, and received the Dipl.-Phys. degree in 1992 and the Ph.D. degree in 1997.

He joined the Institut für Theoretische Elektrotechnik, RWTH Aachen, and in 1995, moved with the group of Prof. B. Meinerzhagen to the Institut für Theoretische Elektrotechnik und Mikroelektronik, Universität Bremen, Germany. Since receiving the Ph.D. degree, he has been with the Institut für Integrierte Systeme, ETH Zürich, Switzerland, working in the field of TCAD on Monte Carlo device modeling and transport theory.

A. Schenk was born in Berlin, Germany, in 1957. He received the Dipl. degree in physics and the Ph.D. in theoretical physics from the Humboldt University Berlin (HUB), in 1981 and 1987, respectively.

In 1987, he became a Research Assistant at the Department of Semiconductor Theory, HUB, and in 1988 he joined the R&D division of WF Berlin. From 1987 to 1991, he worked on various aspects of the physics and simulation of optoelectronic devices, especially infrared detector arrays, and the development and implementation of physical models for modeling infrared sensors. He is now with the Integrated Systems Laboratory, Swiss Federal Institute of Technology, Zurich, Switzerland, as a Senior Lecturer. His main activities are in the development of physics-based models for simulation of submicron silicon devices.

Dr. Schenk is a member of the German Physical Society.

Wolfgang Fichtner (M'79–SM'84–F'90) received the Dipl.Ing. degree in physics and the Ph.D. degree in electrical engineering from the Technical University (TU) of Vienna, Austria, in 1974 and 1978, respectively.

From 1975 to 1978, he was an Assistant Professor in the Department of Electrical Engineering, TU Vienna. From 1979 to 1985, he was with AT&T Bell Laboratories, Murray Hill, NJ. Since 1985, he has been Professor and Head of the Integrated Systems Laboratory , Swiss Federal Institute of Technology, Zurich. In 1993, he founded ISE Integrated Systems Engineering AG, a company in the field of technology CAD.

Dr. Fichtner is a member of the Swiss National Academy of Engineering.